Selection of Metal Oxide Charge Transport Layers for Colloidal Quantum Dot LEDs

V. Wood,* M. J. Panzer, J. E. Halpert, J.-M. Caruge, M. G. Bawendi, and V. Bulović

Department of Electrical Engineering and Computer Science, Department of Chemistry, Massachusetts Institute of Technology, Cambridge, Massachusetts 02139

ARTICLE

ABSTRACT We investigate the effect of the electronic energy level positioning, conductivity, and morphology of metal oxide charge transport layers on the performance of light emitting devices (LEDs) that consist of a colloidally synthesized quantum dot (QD) luminescent film embedded between electron and hole injecting ceramic layers. We demonstrate that understanding of these material properties and their effect on charging processes in QDs enables the systematic design of higher efficiency QD-LEDs and excitation of QDs with different emission colors using the same device structure.

KEYWORDS: quantum dots · electroluminescence · photoemission spectroscopy

Light emitting devices (LEDs) that utilize colloidal quantum dots (QDs) as luminescent centers have generated considerable interest for applications such as thin film displays with improved color saturation and white lighting with high color rendering index. These applications, in particular, require device architectures suitable for electrically exciting different color QDs at comparable input powers. To date, QD-LED demonstrations used semiconducting polymers, molecular organics, and ceramics as charge transport layers, with each material set bringing both benefits and technical challenges.[1−10] The present study extends this line of investigation by considering a series of semiconducting metal oxides in layered QD-LED structures.

Recently we demonstrated that metal oxides can be used as charge transport layers in air-stable QD-LEDs, noting that the efficiency of these structures is significantly reduced by nonradiative processes.[10] First, the relatively high carrier concentrations (typically $\sim 10^{14}/cm^3$) in the p- and n-type metal oxide layers lead to luminescence quenching of the adjacent QDs due to the nonradiative energy transfer between the QDs and the charge-rich metal oxide films.[11,12] Second, the energy band alignment of the component materials impacts the balance between holes and electrons injected into the QD layer, influencing the efficiency of QD-LED operation. For example, in the first demonstration of a metal oxide-based QD-LED structure[10] injection of holes from the p-type NiO into the QD layer was more difficult than electron injection from the n-type zinc tin oxide (ZTO) causing a significant build-up of electrons at the emissive QD multilayer, located between the two ceramics. Such charging of the QDs can lead to an increase in the Auger nonradiative recombination[13−15] decreasing the device efficiency. In this study we show that p- and n-type inorganic charge transport thin films can be systematically selected to counteract the charging processes that cause inefficiency in metal-oxide-based QD-LEDs and demonstrate red, green, and blue QD emission in all-inorganic electrically pumped structures.

RESULTS AND DISCUSSION

In a QD-LED structure, layer morphology, electronic conductivity, and energy band alignment with neighboring layers all affect device performance and can be modified to improve the device quantum efficiency. Here, we study morphology with atomic force microscopy (AFM) and X-ray diffraction (XRD); we determine sheet resistance and carrier concentrations with Van der Pauw and Hall effect measurements; and we use ultraviolet photoelectron spectroscopy (UPS) to measure the ionization energy (IE) of the ceramic layers and of the QD films.

For the UPS measurements, the samples remain in an inert N_2 environment prior to loading into an Omicron NanoTechnology surface analysis system. Both helium I (21.2 eV) and helium II (40.8 eV) lines from a He-discharge lamp are used for sample

*Address correspondence to vwood@mit.edu.

Received for review August 24, 2009 and accepted October 18, 2009.

Published online November 3, 2009.
10.1021/nn901074r CCC: $40.75

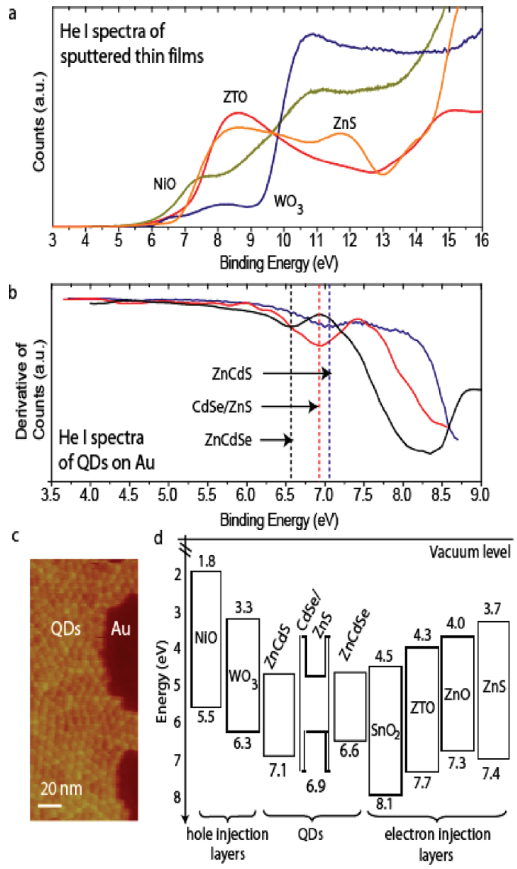

Figure 1. (a) Plot of the He I ultraviolet photoelectron spectroscopy (UPS) measurements on NiO, WO_3, ZTO, and ZnS thin films. (b) Plot of the derivative of the He I UPS spectra for several QD samples. The first minimum of these curves (indicated by the dashed lines) corresponds to the ionization energy of the sample. (c) Atomic force microscopy (AFM) phase image of the edge of a ZnCdSe QD film stamped onto an ultrasmooth template stripped Au surface in preparation for UPS measurements. Individual QDs can be resolved in this image. (d) Band structure of the measured thin films are composed from the UPS measurements of the ionization energy and the optical gap determined by optical absorption measurements.

excitation. For accuracy, 10 scans with 0.02 eV increments are taken in succession and averaged. Figure 1a shows the He I spectra for the sputtered, 20 nm thick ceramic thin films deposited on conductive ITO, as detailed in the Materials and Methods. The IE corresponds to the location of the lowest binding energy inflection point on the UPS data. We measure IEs of (5.5 ± 0.1) eV, (6.3 ± 0.1) eV, (7.3 ± 0.1) eV, and (8.1 ± 0.1) eV for the NiO, WO_3, ZnO, and SnO_2 films, respectively. We note that the cosputtered ZnO and SnO_2 film (ZTO) has an ionization energy of (7.7 ± 0.1) eV, in between that of the constituent ZnO and SnO_2 films.

To clearly show the IE values of different QDs, Figure 1b plots the first derivative of the counts of the He I UPS spectra *versus* the binding energy, such that the local minimum corresponds to the valence band edge. We find values of (7.1 ± 0.2) eV, (6.9 ± 0.2) eV, and (6.6 ± 0.1) eV for the ZnCdS, CdSe/ZnS, and ZnCdSe QDs, respectively. The 6.9 eV value for the core/shell CdSe/ZnS QDs likely represents an average of the ZnS shell and CdSe core contributions to the valence states, which is in agreement with our UPS measurements of ZnS thin films, (7.4 ± 0.1) eV, and CdSe QDs, (6.6 ± 0.1) eV.

While sample preparation for the metal oxide films is relatively straightforward, sample preparation to obtain reproducible UPS measurements on QDs is not trivial, requiring a single complete monolayer of QDs covering an area at least as large as the He I photon beam (here, 2 mm in diameter) on a smooth, conductive substrate. Earlier efforts to prepare films of QDs for UPS measurements involved surface treatments of the QDs to promote adhesion to the metal surface.[16,17] Here, we demonstrate a novel method for depositing a monolayer of QDs on a conductive substrate that does not involve chemical treatment of the QD film, which could alter the band alignment. A film of template stripped Au is prepared following the method described by Blackstock *et al.*[18] The QD solution is then spin-cast onto a parylene-coated polydimethylsiloxane (PDMS) stamp and contact printed[19] onto the metal substrate, leaving a single monolayer of QDs on top of the Au surface. In Figure 1c, the AFM phase image of the edge of a stamped QD film highlights the smooth Au surface and the close-packing of the QD monolayer. This sample preparation method was used to obtain the UPS measurements in Figure 1b and could be implemented with a variety of metal films, having a range of workfunctions, and QDs with different capping groups in order to understand the role of the QD/metal interface on the measured IE values.

The electron affinity (EA) of the materials is calculated by adding the electron energy band gap of each film to the measured ionization energy. We determine the band gaps of the ceramics by measuring the absorption onset of their thin films on quartz using a CARY 500i spectrophotometer. An approximate band gap of the QDs is obtained by measuring their photoluminescence (PL) spectrum and assuming an additional 100 meV to account for the approximate Stokes shift of the PL peak with respect to the optical absorption edge.[20] The IE and EA data for materials used in this study are summarized in Figure 1d.

We next provide examples of how a detailed understanding of the structural and electronic properties of the component metal oxides and the QD emissive layers is critical to the design and fabrication of efficient QD-LEDs. While there have been reports of other types of metal-oxide-based QD-LEDs,[21−23] here we focus exclusively on possible improvements to the device architecture in which QDs are sandwiched between radio frequency sputtered hole and electron injecting metal oxide layers. Details regarding the deposition conditions of each layer can be found in the Materials and Methods, but an overview of the device fabrication is provided here. All devices use commercial ITO-coated

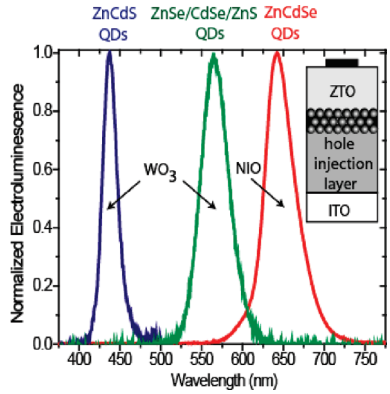

Figure 2. Electroluminescence spectra of blue, green, and red-emitting QDs in metal-oxide based QD-LEDs. WO_3 hole injection layer is used for blue and green QD-LEDs, while NiO was used in red[10] QD-LEDs. The spectra are taken at 18, 15, and 12 V for the blue, green, and red devices, respectively.

glass substrates (produced by Thin Films, Inc.) as the anode. RF magnetron sputtering is chosen as the deposition method for the metal oxide transport layers since it is a physical vapor deposition (*i.e.*, nonreactive) technique that can be performed at low power and at room temperature. The hole injection layer is deposited first, followed by the QDs, the electron injection layer, and finally the cathode (see device schematic in the inset of Figure 2). QDs are spun-cast onto the hole injection layer from solution. The thickness of the spin-cast layer is calibrated to obtain (4+/−1) monolayers of QDs using AFM measurements. The electron injection layer (ZTO) is sputter-deposited using Ar plasma to minimize the O_2 exposure of the QD film. The top contact is a 100 nm thick film of either sputtered ITO or an evaporated metal (such as Ag, Au, or Al). Each 12 mm by 12 mm substrate has 10 devices (1 mm by 2 mm), which are defined by the top electrodes. All devices are tested unpackaged and in air.

Use of QDs as the luminescent color centers in multicolor displays or mixed color white lighting requires excitation of red, green, and blue QDs as a minimum.[24] However, the operating efficiency of QD-LEDs with metal oxide charge transport layers is sensitive to the QD/metal oxide energy band alignment, making multicolor QD excitation particularly challenging.

Monochrome light emission across the entire visible spectrum can be generated with the standard CdSe/ZnS core−shell QD. However, the luminescence efficiency of these CdSe/ZnS QDs is not very high in the deep red or in the blue part of the spectrum.[4] The ZnCdSe QDs can be made as efficient deep-red lumophores, and have been used in the initial device demonstration,[10] but they are not suitable for wavelengths shorter than $\lambda = 560$ nm. Previous work has shown that stable and efficient blue-emitting QDs can be obtained with a ZnCdS alloyed core.[4] The UPS data summarized in Figure 1d show that the valence band of ZnCdS is at 7.1 eV, which is 0.5 eV lower in energy than the valence band of the ZnCdSe QDs used in the initial metal oxide-based QD-LED device. Since the holes already face a 1.1 eV barrier to injection from NiO into the ZnCdSe QDs, it is not surprising that we observed no electroluminescence (EL) from blue-emitting ZnCdS QDs when they replace the red-emitting ZnCdSe QDs in a NiO/QD/ZTO device structure. To demonstrate that this is, indeed, the result of the increased energy band offset, we replace the NiO layer with a WO_3 layer that is reported to improve hole injection[25] with an IE located 0.8 eV below that of NiO. The EL spectra in Figure 2 show the blue ZnCdS and green ZnSe/CdS/ZnS QD emission is made possible by the replacement of NiO with WO_3.

These results demonstrate that energy band alignment between the metal oxides and the luminescent QD film is critical for efficient device operation. However, transport layers can be further improved beyond energy band alignment with the QDs. As noted earlier, we identified two important contributors to reduced device operating efficiency: charging of the QD layer and the conductivity of the adjacent metal oxide layer. The ZTO layer already offers favorable band alignment so we demonstrate changes that can be made to the ZTO to address these two sources of inefficiency.

Figure 3a presents the cross sectional schematics of four inorganic QD-LED device architectures. Structures 2−4 indicate different ways to improve the efficiency of the basic NiO/QD/ZTO device (Structure 1). Current density versus voltage ($J-V$) and external quantum efficiency (EQE) trends for the four structures are shown in Figure 3b. The series of four devices were fabricated and tested a total of five times. Each time, the four devices were processed in parallel to ensure uniformity between layers shared by the four devices. Different batches of ZnCdSe QDs were used for the five different devices series, resulting in some variation in the absolute EQE values. However, the trends in $J-V$ and EQE remained the same for each series of four devices, so here we present the EQE data as averages of the five different device series. The average EQEs are normalized with respect to the average EQE of Structure 1, and the largest EQE for Structure 4 observed was 0.2%.

The first method for increasing device efficiency is to decrease the amount of QD luminescence quenching due to free carriers in the adjacent metal oxide layers. We are focused on improving the electron transport layer, which is located on top of the QDs. To reduce quenching, we deposit a thin, relatively insulating layer in an Ar environment at low power to avoid additional damage to the QD film. We choose a 10 nm thick layer of insulating ZnO on top of the QDs (Structure 2). The particular growth conditions that enable nearly stochiometric (and therefore insulating) ZnO to be deposited in an Ar environment are described in detail in the Materials and Methods. The EQE plot shows that the addition of the 10 nm-thick ZnO layer correspondingly boosts EQE by a factor of 2. To confirm that this increase in EQE is related to the decrease in QD lumines-

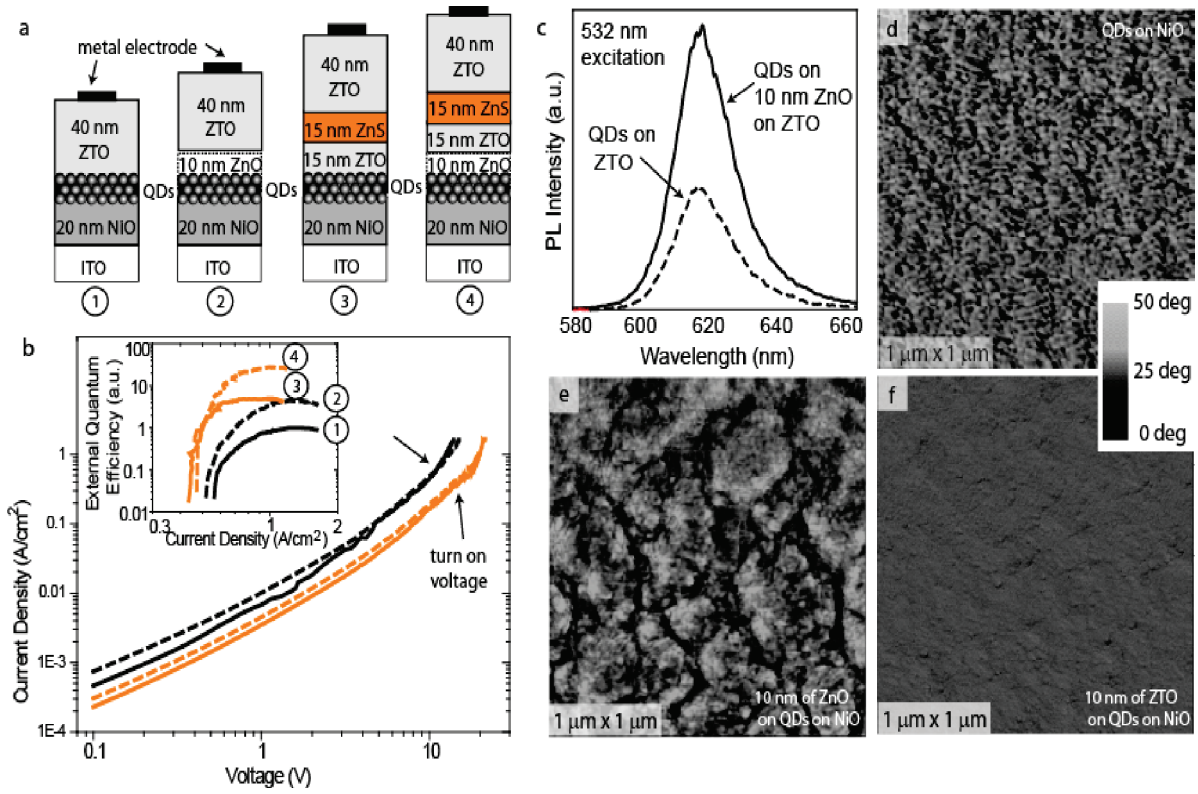

Figure 3. (a) Schematics of the NiO-QD-ZTO device structures with modified n-type transport layers. In Structures 2 and 4, a 10 nm-thick layer of ZnO is sputtered on top of the spin-cast QD film. Structures 3 and 4 contain a 15 nm-thick layer of ZnS within the ZTO. (b) Current density *vs* voltage (*J*−*V*) characteristics of the four structures. The addition of the ZnO layer (dashed *versus* solid lines) does not increase the turn on voltage of the devices. The inset plot of the EQE as a function of current density shows systematic improvement across the four structures. The EQE characteristics for each structure are an average of data from five sets of devices, with each of the four structures processed in parallel for a given set. (c) Photoluminescence spectra of QDs excited with a λ = 532 nm laser. The film of QDs is spin-cast on either a 40 nm thick layer of sputter deposited ZTO (dashed line) or 10 nm of ZnO on top of 40 nm of ZTO (solid line). The addition of 10 nm of insulating ZnO doubles the PL response of the QD film. AFM phase images measurements showing the QDs spin-cast onto the NiO (d), 10 nm of ZnO sputter-deposited on the QD film (e), and 10 nm of ZTO sputter-deposited on the QD film (f).

cence quenching, we spin a highly dilute solution of QDs to form a submonolayer of QDs on either ZTO or 10 nm-thick film of ZnO on ZTO. Figure 3c compares the photoluminescence (PL) of these two samples with (solid line) and without (dashed line) a ZnO layer adjacent to the QDs. A λ = 532 nm laser source is used so that only the QDs—and not the metal oxides—are optically excited. Consistency between PL measurements for different samples is ensured by using a microscope objective to uniformly illuminate and collect luminescence from the entire sample area. The PL spectra reveal two times higher QD luminescence intensity over the integrated area for the sample with the ZnO layer, indicating that the insertion of this layer reduced the number of free carriers near the QD layer and the amount of luminescence quenching.

We note that even though ZnO is an insulating layer, the turn-on voltage remains 6 V for both Structures 1 and 2. We attribute this to the fact that the ZnO does not completely cover the QD layer, as seen by comparing the AFM phase images of the initial QD film (Figure 3d), 10 nm of ZnO on top of the QDs (Figure 3e), and 10 nm of ZTO on top of the QDs (Figure 3f). The incomplete ZnO layer enables passage of charge through the cracks, but still minimizes the concentration of charge carriers adjacent to the QDs.

The second source of luminescence quenching is charging of the QD film. Figure 1d shows that there is no energy barrier to electron injection into the ZnCdSe QDs from the ZTO, which leads to build-up of electrons in the QD film. Structure 3 demonstrates that inserting a 15 nm-thick layer of RF sputtered ZnS within the ZTO layer improves the EQE by a factor of 5 over that of Structure 1. As shown in Figure 1d, wide band gap, insulating ceramic ZnS presents a 0.6 eV energy barrier to electron transport in the ZTO layer, and can be used to balance the number of electrons and holes arriving at the QD layer. Since sputtered ZnS does not deposit uniformly on the QDs, in order to ensure a smooth and continuous layer, the ZnS is deposited on top of a low roughness ZTO film (See Figure 3f) that is deposited on top of the QD film first (15 nm in thickness). We note that the insertion of the insulating ZnS layer increases the turn on of the device from 6 to 11 V (Figure 3b). ZnO is an insulating layer, but it only offers a 0.3 eV energy barrier to electron flow in the ZTO and, as described

above, it does not form a continuous layer across the QD film. Thus the ZnO layer serves primarily to reduce QD luminescence quenching, while the ZnS layer limits QD charging by reducing electron injection into the QD film. The presence of both a 10 nm-thick ZnO layer and a 15 nm ZnS layer (Structure 4) results in the most efficient of the four device structures presented and again does not further increase the turn on voltage of the device beyond 11 V.

CONCLUSIONS

In summary, we demonstrate that an understanding of the electronic and structural properties of the component materials in metal-oxide-based QD-LEDs enables systematic fabrication of devices that exhibit increased efficiency and multicolor EL. At the same time, this work underscores the importance of rethinking the design of thin-film QD-LEDs. Organic-based QD-LEDs hold the record efficiencies because of the important role of Förster energy transfer and the need for only a single monolayer of QDs.[26] Hybrid QD-LEDs with inorganic and organic transport layers can benefit from the dual excitation mechanisms of Förster energy transfer and direct charge injection while gaining stability from the ceramic materials. Systematic improvements to efficiency are possible in the case of inorganic QD-LEDs that operate *via* direct charge injection, but ultimately new methods for excitation of colloidal QDs that reduce nonradiative charging processes and do not require energy band alignment[21−23,27] should be investigated.

MATERIALS AND METHODS

The QDs used in this work are the same as those described in Anikeeva *et al*.[4] The red-emitting ZnCdSe cores, synthesized following the process described in Zhong *et al*.,[28] are capped with oleic acid and have a PL peak at $\lambda = 632$ nm and a solution PL quantum yield of 50%. The green-emitting ZnSe/CdSe/ZnS core-double-shell QDs, passivated with hexylphosphonic acid and TOPO, are synthesized with a technique similar to those reported by Ivanov *et al*.[29] and Steckel *et al*.[30] and have a PL peak at $\lambda = 540$ nm and a solution PL quantum yield of 65%. The ZnCdS cores are passivated with oleic acid and oleylamine and are synthesized following the work of Zhong *et al*.[31] The PL peak is at $\lambda = 460$ nm and the solution PL quantum yield is 50%. The CdSe/ZnS core−shell structures studied with UPS follow the synthesis in Daboussi *et al*.[32] The QDs are precipitated from the growth solution using acetone, redispersed in hexane, precipitated a second time using methanol and butanol, and finally redispersed in chloroform prior to spin-casting on the p-type metal oxide layer at 1200 rpm. The solution processing steps are performed in a N_2 glovebox.

The ceramic layers are RF magnetron sputtered in a custom-built system outfitted with US Inc. sources, and the three-inch diameter, hot-pressed targets of NiO, WO_3, ZnO, SnO_2, and ZnS are purchased from Plasmaterials, Inc. The NiO is sputtered at 200 W with a 30:1 Ar/O_2 volume ratio at 6 mTorr chamber pressure. The WO_3 is sputtered at 60 W with a 10:1 Ar/O_2 volume ratio. In the case of WO_3, it is desirable to deposit a layer with graded conductivity by gradually increasing the O_2 partial pressure during the deposition process so that the least conductive part of the WO_3 layer is closest to the QD layer. This is analogous to the method for improving the efficiency implemented in Structure 2, where a layer of 10 nm-thick ZnO is placed between the ZTO and QD film. To form a highly insulating ZnO layer, the ZnO target is presputtered to be stochiometric prior to introducing the sample with the exposed QD film. The ZnO film is then sputter-deposited at 16 W in an Ar environment at 4 mTorr to prevent damage to the QD layer. While the ZnO becomes progressively nonstochiometric during sputtering at these conditions, we find that a 10 nm-thick layer remains sufficiently insulating and note that the most insulating section of the ZnO is in contact with the QD layer. The ZTO layer is prepared by cosputtering the ZnO and SnO_2 at 9 and 15 W, respectively, in a 4 mTorr Ar environment. The ZnS layer is sputtered at 35 W in Ar at 4 mTorr.

Our devices are measured without environmental packaging and in atmospheric conditions. Current $J-V$ characteristics of the QD-LEDs are recorded using a computer controlled Keithley 2602 current/voltage source-meter. To calculate the EQEs, the EL from the front face of the device is detected using a calibrated Newport 818-UV silicon photodetector at the same time that the $J-V$ characteristics are measured. EL spectra are taken with an Acton spectrometer with bias applied to the device using the Keithley 2602.

Acknowledgment. This work is supported by the Institute for Soldier Nanotechnologies (DAAD-19-02-0002), a Presidential Early Career Award for Scientists and Engineers (V. Bulović), and a National Defense Science and Engineering Graduate Fellowship (V. Wood). This work made use of MRSEC Shared Experimental Facilities at MIT, supported by the National Science Foundation under award DMR-02-13282.

REFERENCES AND NOTES

1. Colvin, V. L.; Schlamp, M. C.; Alivisatos, A. P. Light-Emitting-Diodes Made from Cadmium Selenide Nanocrystals and a Semiconducting Polymer. *Nature* **1994**, *370*, 354–357.
2. Coe, S.; Woo, W. K.; Bawendi, M. G.; Bulović, V. Electroluminescence from Single Monolayers of Nanocrystals in Molecular Organic Devices. *Nature* **2002**, *420*, 800–803.
3. Zhao, J.; Bardecker, J. A.; Munro, A. M.; Liu, M. S.; Niu, Y.; Ding, I.-K.; Luo, J.; Chen, B.; Jen, A. K.-Y.; Ginger, D. S. Efficient CdSe/CdS Quantum Dot Light-Emitting Diodes Using a Thermally Polymerized Hole Transport Layer. *Nano Lett.* **2006**, *6*, 463–467.
4. Anikeeva, P. O.; Halpert, J. E.; Bawendi, M. G.; Bulović, V. QD-LEDs with Electroluminescence Tunable over the Entire Visible Spectrum. *Nano Lett.* **2009**, *9*, 2532–2536.
5. Cho, K.-S.; Lee, E. K.; Joo, W.-J.; Jang, E.; Kim, T.-H.; Lee, S. J.; Kwon, S.-J.; Han, J. Y.; Kim, B.-K.; Choi, B. L.; *et al.* High-Performance Crosslinked Colloidal Quantum-Dot Light-Emitting Diodes. *Nat. Photonics* **2009**, *3*, 341–345.
6. Caruge, J.-M.; Halpert, J. E.; Bulović, V.; Bawendi, M. G. NiO as an Inorganic Hole-Transporting Layer in Quantum-Dot Light-Emitting Devices. *Nano Lett.* **2006**, *6*, 2991–2994.
7. Bolink, H. J.; Coronado, E.; Repetto, D.; Sessolo, M. Air Stable Hybrid Organic−Inorganic Light Emitting Diodes Using ZnO as the Cathode. *Appl. Phys. Lett.* **2007**, *91*, 223501.
8. Stouwdam, J. W.; Janssen, R. A. J. Red, Green, And Blue Quantum Dot LEDs with Solution Processable ZnO Nanocrystal Electron Injection Layers. *J. Mater. Chem.* **2008**, *18*, 1889–1894.
9. Mueller, A. H.; Petruska, M. A.; Achermann, M.; Werder, D. J.; Akhadov, E. A.; Koleske, D. D.; Hoffbauer, M. A.; Klimov, V. I. Multicolor Light-Emitting Diodes Based on Semiconducting Nanocrystals Encapsulated in GaN Charge Injection Layers. *Nano Lett.* **2005**, *5*, 1039.

10. Caruge, J.-M.; Halpert, J. E.; Wood, V.; Bawendi, M. G.; Bulović, V. Colloidal Quantum-Dot Light-Emitting Diodes with Metal-Oxide Charge Transport Layers. *Nat. Photonics* **2008**, *2*, 247–250.
11. Chance, R. R.; Prock, A.; Silbey, R. J. Molecular Fluorescence and Energy Transfer Near Interfaces. *Adv. Chem. Phys.* **1978**, *37*, 1.
12. Shimizu, K. T.; Woo, W. K.; Fisher, B. R.; Eisler, H. J.; Bawendi, M. G. Surface-Enhanced Emission from Single Semiconductor Nanocrystals. *Phys. Rev. Lett.* **2002**, *89*, 117401–117404.
13. Nirmal, M.; Dabbousi, B. O.; Bawendi, M. G.; Macklin, J. J.; Trautman, J. K.; Harris, T. D.; Brus, L. Fluorescence Intermittency in Single Cadmium Selenide Nanocrystals. *Nature* **1996**, *383*, 802–804.
14. Efros, A. L.; Rosen, M. Random Telegraph Signal in the Photoluminescence Intensity of a Single Quantum Dot. *Phys. Rev. Lett.* **1997**, *78*, 1110–1113.
15. Tang, J.; Marcus, R. A. Diffusion-Controlled Electron Transfer Processes and Power-Law Statistics of Fluorescence Intermittency of Nanoparticles. *Phys. Rev. Lett.* **2005**, *95*, 107401.
16. Colvin, V. L.; Goldstein, A. N.; Alivisatos, A. P. Semiconductor Nanocrystals Convalently Bound to Metal-Surfaces with Self-Assembled Monolayers. *J. Am. Chem. Soc.* **1992**, *114*, 5221–5230.
17. Wu, P.-J.; Tsuei, K. D.; Hsieh, M.-T.; Wei, K.-H.; Liang, K. S. Dependence of the Final-State Effect on the Coupling between a CdSe Nanoparticle and Its Neighbors Studied with Photoemission Spectroscopy. *Phys. Rev. B* **2007**, *75*, 115402.
18. Blackstock, J. J.; Li, Z.; Freeman, M. R.; Stewart, D. R. Ultra-Flat Platinum Surfaces from Template-Stripping of Sputter Deposited Films. *Surf. Sci.* **2003**, *546*, 87–96.
19. Kim, L.; Anikeeva, P. O.; Coe-Sullivan, S. A.; Steckel, J. S.; Bawendi, M. G.; Bulović, V. Contact Printing of Quantum Dot Light-Emitting Devices. *Nano Lett.* **2008**, *8*, 4513–4517.
20. Meulenberg, R. W.; Lee, J. R. I.; Wolcott, A.; Zhang, J. Z.; Terminello, L. J.; von Buuren, T. Determination of the Excition Binding Energy in CdSe Quantum Dots. *ACS Nano* **2009**, *3*, 325–330.
21. Achermann, M.; Petruska, M. A.; Koleske, D. D.; Crawford, M. H.; Klimov, V. I. Nanocrystal-Based Light-Emitting Diodes Utilizing High-Efficiency Nonradiative Energy Transfer for Color Conversion. *Nano Lett.* **2006**, *6*, 1396–1400.
22. Kobayashi, S.; Tani, Y.; Kawazoe, H. Quantum Dot Activated All-Inorganic Electroluminescent Device Fabricated Using Solution-Synthesized CdSe/ZnS Nanocrystals. *Jpn. J. Appl. Phys.* **2007**, *46*, L966–L969.
23. Wood, V.; Panzer, M. J.; Caruge, J.-M.; Halpert, J. E.; Bawendi, M. G.; Bulović, V. submitted for publication, 2009.
24. Anikeeva, P. O.; Halpert, J. E.; Bawendi, M. G.; Bulović, V. Electroluminescence from a mixed red-green-blue colloidal quantum dot monolayer. *Nano Lett.* **2007**, *7*, 2196–2200.
25. Meyer, J.; Winkler, T.; Hamwi, S.; Schmale, S.; Johannes, H.-H.; Weimann, T.; Hinze, P.; Kowalsky, W.; Riedl, T. Transparent Inverted Organic Light-Emitting Diodes with a Tungsten Oxide Buffer Layer. *Adv. Mater.* **2008**, *20*, 3839–3843.
26. Anikeeva, P. O.; Madigan, C. F.; Halpert, J. E.; Bawendi, M. G.; Bulović, V. Electronic and Excitonic Processes in Light-Emitting Devices Based on Organic Materials and Colloidal Quantum Dots. *Phys. Rev. B* **2008**, *78*, 085434.
27. Wood, V.; Panzer, M. J.; Chen, J. L.; Bradley, M. S.; Halpert, J. E.; Bawendi, M. G.; Bulović, V. Inkjet-Printed Quantum Dot-Polymer Composites for Full-Color AC-Driven Displays. *Adv. Mater.* **2009**, *21*, 2151–2155.
28. Zhong, X.; Han, M.; Dong, Z. h.; White, T.; Knoll, W. Composition-Tunable $Zn_xCd_{1-x}Se$ Nanocrystals with High Luminescence and Stability. *J. Am. Chem. Soc.* **2003**, *125*, 8589–8594.
29. Ivanov, S. A.; Nanda, J.; Piryatinski, A.; Achermann, M.; Balet, L. P.; Bezel, I. V.; Anikeeva, P. O.; Tretiak, S. T.; Klimov, V. Light Amplification Using Inverted Core/Shell Nanocrystals: Towards Lasing in the Single-Exciton Regime. *J. Phys. Chem.* **2004**, *108*, 10625–10630.
30. Steckel, J. S.; Steckel, J. S.; Snee, P.; Coe-Sullivan, S.; Zimmer, J. P.; Halpert, J. E.; Anikeeva, P.; Kim, L.-A.; Bulović, V.; Bawendi, M. G. Color-Saturated Green-Emitting QD-LEDs. *Angew. Chem., Int. Ed.* **2006**, *45*, 5796–5799.
31. Zhong, X.; Feng, Y.; Knoll, W.; Han, M. Alloyed $Zn_xCd_{1-x}S$ Nanocrystals with Highly Narrow Luminescence Spectral Width. *J. Am. Chem. Soc.* **2003**, *125*, 13559–13563.
32. Dabbousi, B. O.; Rodriguez-Viejo, J.; Mikulec, F. V.; Heine, J. R.; Mattoussi, H.; Ober, R.; Jensen, K. F.; Bawendi, M. G. (CdSe)ZnS Core-Shell Quantum Dots: Synthesis and Characterization of a Size Series of Highly Luminescent Nanocrystallites. *J. Phys. Chem. B.* **1997**, *101*, 9463–9475.